JOURNAL OF APPLIED POLYMER SCIENCE VOL. 18, PP. 1319–1350 (1974)

Fracture Response of Polyimide and Polysulfone under Hydrostatic Pressure

S. K. BHATEJA, K. D. PAE, and J. A. SAUER,
Department of Mechanics and Materials Science, Rutgers University, New Brunswick, New Jersey 08903

Synopsis

Fracture response of polyimide and polysulfone in tension under superimposed hydrostatic pressures up to 100,000 psi is presented. The influence of hydrostatic pressure and the pressure medium on the specific surface energy γ is determined by utilizing the Griffith theory of brittle fracture. For polyimide as well as for polysulfone, γ is found to increase with increasing pressure. Furthermore, for polysulfone at any given pressure level, the value of γ is found to be lower in heptane medium than in kerosene. Heptane is known to be a stress-cracking agent for polysulfone. Fracture surface of the tested tensile specimens is examined by using a scanning electron microscope. The observed fracture features are correlated with the macroscopic deformation behavior and also with the effects of the pressure medium used. In polyimide, the region of crack initiation narrows down from a very broad region at atmospheric pressure to almost a point source along the outer periphery of the specimen at 100,000 psi. In addition, polyimide undergoes a transition in the nature of fracture response between 80,000 to 100,000 psi, and this is clearly indicated in the scanning electron micrographs. In polysulfone, the crack propagation appears to be faster when heptane is used as the pressure medium than when kerosene is used. The penetration of the medium into the specimens can be observed on the micrographs. Several scanning electron micrographs of the fracture surface suggest the possibility of a significant temperature rise in the specimen during fracture. This increase in the specimen temperature is roughly estimated from the stored elastic energy released upon fracture.

INTRODUCTION

The elastic and plastic stress–strain behavior of polyimide and polysulfone under hydrostatic pressure has already been published in detail.[1–3] The purpose of this paper is to report on the fracture response of these materials under hydrostatic pressure. Fracture surfaces of tested tensile specimens have been examined by scanning electron microscopy to achieve a better insight into the nature of the fracture process and also to investigate the influence of pressure and the pressure medium on the fracture behavior. Attempts are made to correlate the observed fracture features with the reported macroscopic fracture and deformation behavior and with the structure of each polymer. The Griffith theory of brittle fracture is utilized to estimate, from the experimental data, the variation of specific "surface energy" with hydrostatic pressure. Possible reasons for the

difference in the magnitude of the observed and the theoretical values of the specific surface energy are considered.

STRESS–STRAIN BEHAVIOR OF POLYIMIDE AND POLYSULFONE UNDER HYDROSTATIC PRESSURE

The principle features associated with the deformation and fracture response of polyimide and polysulfone specimens will now be briefly reviewed. Figure 1 shows the nominal tensile stress–strain curves of polyimide under various superimposed hydrostatic pressures up to 100,000 psi. The elastic modulus, as measured by the initial slope of these curves, and the fracture strength both increased with increasing pressure. More striking features, however, are the significant increase in ductility (measured by the elongation to fracture) that occurs at higher pressures and the occurrence of a definite tensile yield maximum at a hydrostatic pressure of 100,000 psi in this normally brittle material.

Figure 2 shows a set of polyimide tensile specimens that have been fractured at the various pressure intensities indicated. The specimen tested at atmospheric pressure fractures in a rather brittle manner, the nominal fracture strain being less than 10%. There is no indication of localized necking, and the fracture surface is sharp and essentially normal to the direction of the applied tensile stress. A neck, however, begins to appear in the specimen when the pressure reaches about 80,000 psi, and the neck becomes further developed at a pressure of 100,000 psi. At this pressure, a considerable amount of localized deformation and shearing occurs and

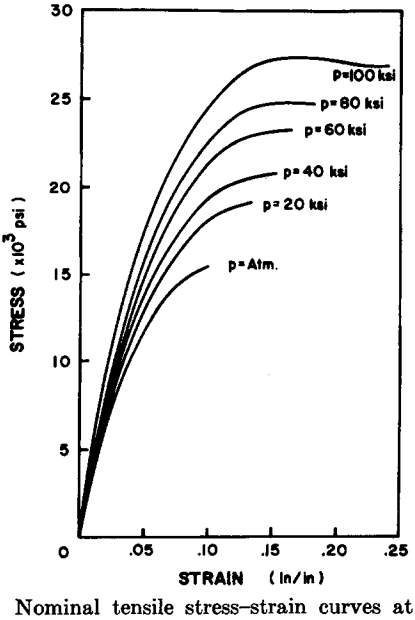

Fig. 1. Polyimide. Nominal tensile stress–strain curves at various pressures.

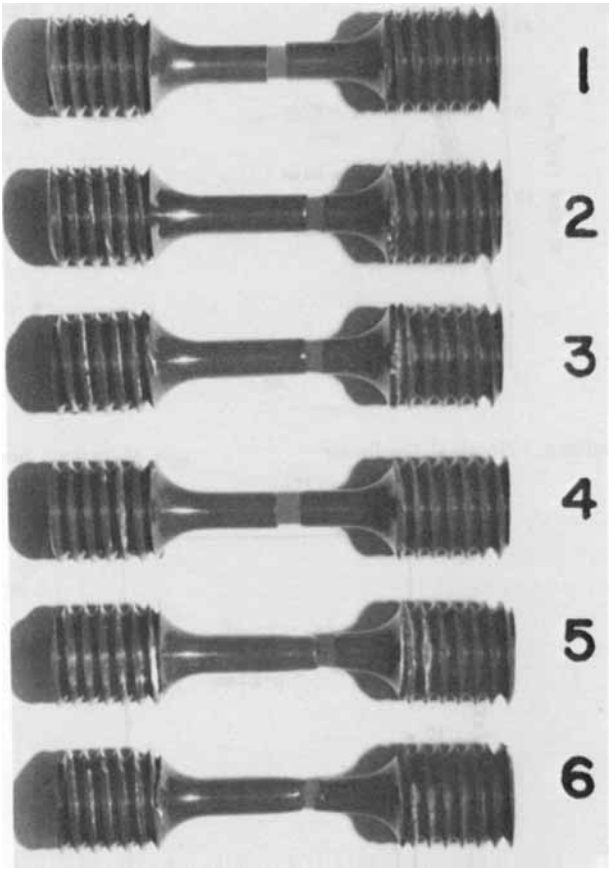

Fig. 2. Polyimide. Photograph of typical tensile specimens tested at (1) atmospheric pressure; (2) 20,000 psi; (3) 40,000 psi; (4) 60,000 psi; (5) 80,000 psi; (6) 100,000 psi.

the plastic deformation prior to fracture reaches about 25%. Also, the fracture surface is now no longer perpendicular to the tensile load direction but is quite jagged.

The nominal tensile stress–strain curves of conventionally extruded, and subsequently annealed, specimens of polysulfone tested in kerosene oil as the pressure medium are shown in Figure 3. Again, it is apparent from these curves that the tensile modulus, the fracture strength, and the nominal ductility tend to increase with increasing pressure. However, the most interesting feature of these data is the occurrence of a pressure-induced brittle–ductile transition between pressures of 40,000 and 60,000 psi. At and below, 40,000 psi, the specimens fracture in an essentially brittle manner, with no indication of any localized necking. Above this pressure level, however, the specimens exhibit a ductile response, the tensile stress–strain curves showing the presence of both an upper and a lower yield point followed by a region of almost perfectly platic flow. The nominal fracture strain increases from about 6% when tests are made on these

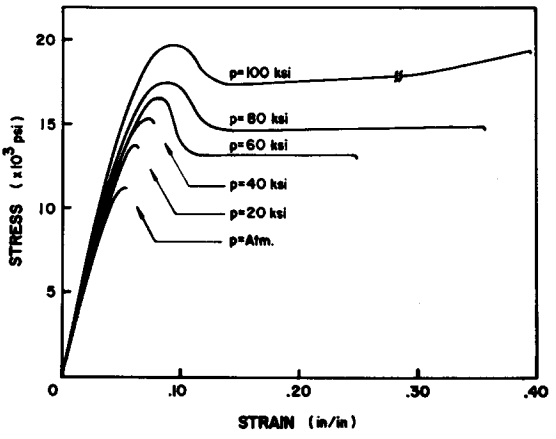

Fig. 3. Polysulfone. Nominal tensile stress–strain curves at various pressures (kerosene).

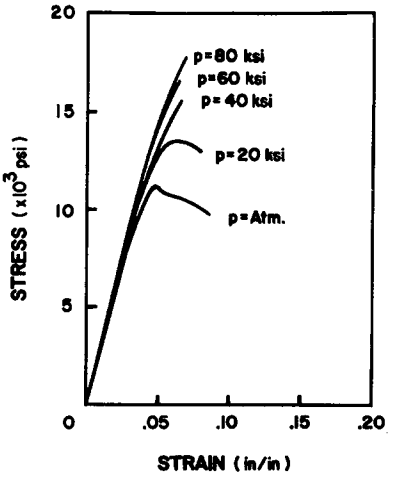

Fig. 4. Polysulfone. Nominal tensile stress–strain curves at various pressures (heptane).

samples at atmospheric pressure, to about 47% for tensile tests carried out at a pressure of 100,000 psi. There is also a sudden large increase in ductility at the transition pressure.

When similar tests are made with heptane instead of kerosene as the pressure-transmitting fluid, the observed tensile behavior of polysulfone is quite different. This is shown in the nominal tensile stress–strain curves of Figure 4. The specimen tested at atmospheric pressure shows limited ductility but exhibits an upper yield point. Correspondingly, the fractured specimen shows some localized necking, Figure 6. The specimen tested at a pressure of 20,000 psi fractures just past the upper yield point. All the specimens tested at and above 40,000 psi pressure fracture in a brittle manner short of the yield point. The nominal fracture strain is about

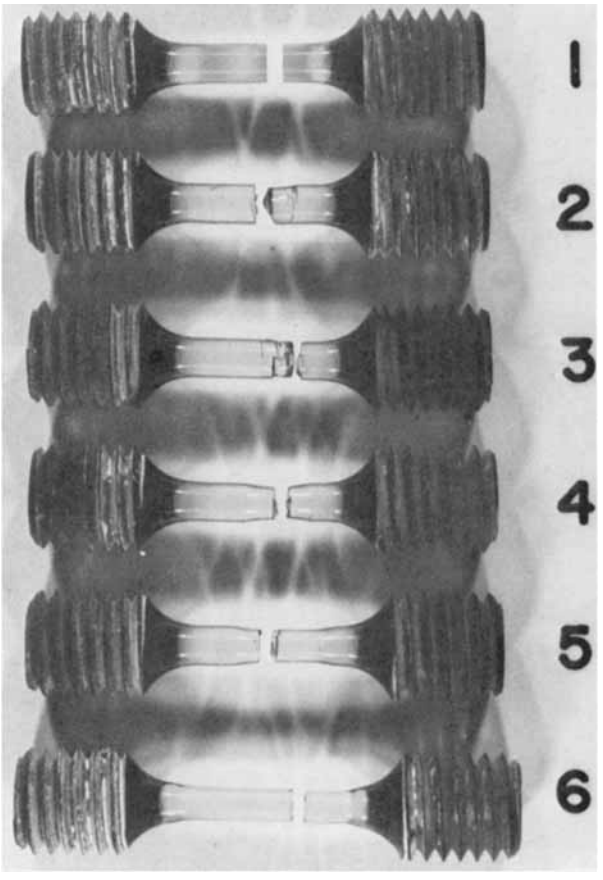

Fig. 5. Polysulfone. Photograph of typical tensile specimens tested in kerosene at (1) atmospheric pressure; (2) 20,000 psi; (3) 40,000 psi; (4) 60,000 psi; (5) 80,000 psi; (6) 100,000 psi.

9% at atmospheric pressure and appears to decrease somewhat with increasing pressure.

A set of fractured polysulfone tensile specimens tested in kerosene oil at different pressures is shown in Figure 5, while the corresponding set of specimens tested in heptane is shown in Figure 6. A comparison of corresponding specimens in these two sets indicates differences in the nature of fracture in the two different test media. While all the specimens, except that at atmospheric pressure, tested in heptane show a brittle fracture, it is only the specimens tested at pressures below 40,000 psi in kerosene oil which show brittleness. The specimens tested at higher pressures in kerosene oil clearly show neck formation and subsequent cold-drawing, and the ductility continues to increase with increasing hydrostatic pressure.

A microscopic examination of the free surface of the specimens tested in both the media reveals that some stress crazing has occurred but that the

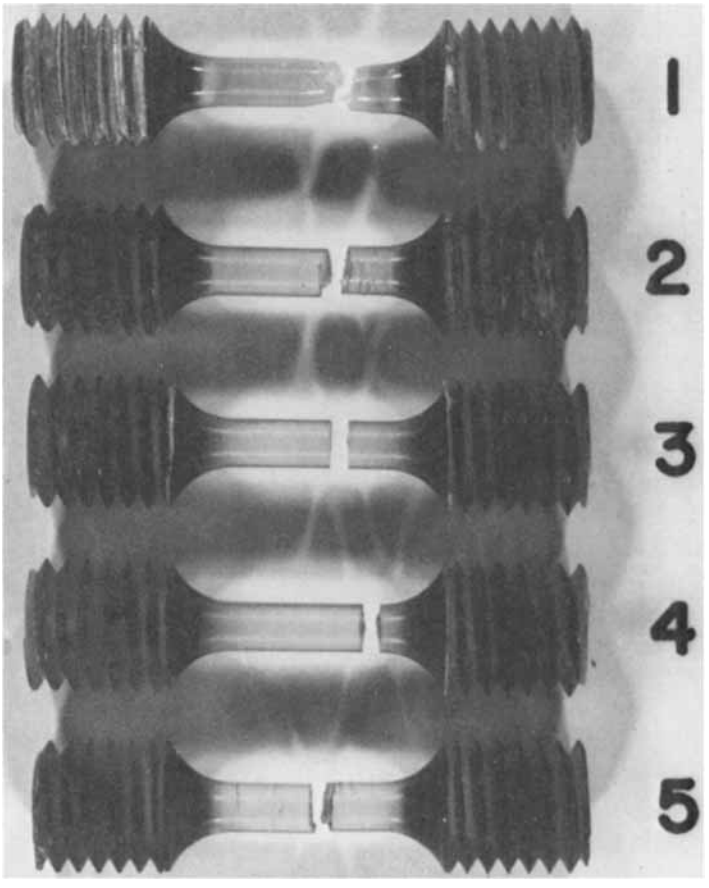

Fig. 6. Polysulfone. Photograph of typical tensile specimens tested in heptane at (1) atmospheric pressure; (2) 20,000 psi; (3) 40,000 psi; (4) 60,000 psi; (5) 80,000 psi.

amount of crazing diminishes with increasing pressure. The crazing "cracks" are much denser and more prominent when heptane is used as the pressure medium than when kerosene oil is used. The specimens tested at 60,000 psi or higher pressure with kerosene oil as the pressure medium no longer show any indication of crazing marks on the free surface. However, when heptane is used as the pressure medium, the crazing "cracks" can still be seen on the free surface of even those specimens that were tested at pressures as high as 80,000 psi.

FRACTURE RESPONSE OF POLYIMIDE AND POLYSULFONE UNDER HYDROSTATIC PRESSURE

Considerations from Griffith Theory of Brittle Fracture

Griffith postulated that an existing crack or flaw would propagate in a brittle material when the elastic, stored energy released by the strained

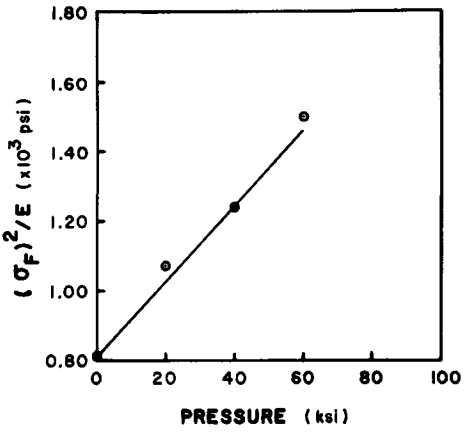

Fig. 7. Polyimide. $(\sigma_F)^2/E$ vs. pressure.

body as a result of an incremental growth of the flaw reached the value required to generate the two new fracture surface increments. He thus derived the following equation:

$$\sigma_F = \sqrt{\frac{2E\gamma}{\pi C}} \tag{1}$$

where σ_F is the nominal stress required to produce brittle fracture, E is the modulus of elasticity of the material, $2c$ is the crack length, and γ is the energy required to create unit surface area.

If E and σ_F are taken to be characteristic constants of a particular material, it is to be expected from eq. (1) that

$$\frac{\sigma_F^2}{E} = \frac{2\gamma}{\pi c} = \text{constant.} \tag{2}$$

In actual situations, eq. (2) has been observed to apply only under special conditions. Several investigators have shown that when deliberate cracks, of varying length $2c$, are introduced, eq. (2) is satisfied by brittle materials. From the experimental data, an approximate value of γ, the energy required to create unit surface area, can be determined. The values of γ thus obtained have been found to greatly exceed theoretically possible values. A discussion of the possible reasons for this discrepancy will be presented later. However, for the purpose of determining the dependence of γ on hydrostatic pressure, eq. (2) will be used in this paper.

From tensile stress–strain data acquired under high pressure conditions, it appears possible to say something definite about the pressure dependence of γ, or at least of the ratio γ/c for the polymers studied. It has been found that both σ_F and E vary significantly with the intensity of hydrostatic pressure P, and so also does the ratio σ_F^2/E. Figure 7, for example, shows how this quantity (σ_F^2/E) varies with P for polyimide. Each datum point in Figures 7 to 9 represents an average of three different values

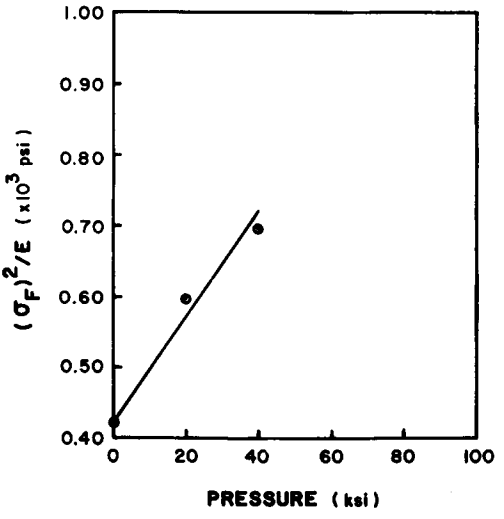

Fig. 8. Polysulfone. $(\sigma_F)^2/E$ vs. pressure (kerosene).

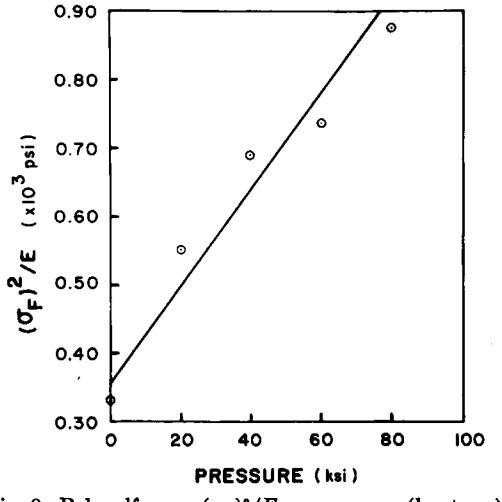

Fig. 9. Polysulfone. $(\sigma_F)^2/E$ vs. pressure (heptane).

obtained at that pressure level. It appears that the relation is almost linear up to about 60,000 psi. The Griffith theory applies only to brittle-type fracture. Polyimide, while perhaps never really brittle in the Griffith sense, nevertheless shows no shear yielding until at pressures above 60,000 psi, where it undergoes a brittle–ductile transition. The (σ_F^2/E)-versus-P plot probably loses significance above this pressure value.

Similar plots for the brittle-fracture region for polysulfone specimens, fractured in a kerosene oil medium and in a heptane medium, are shown in Figures 8 and 9, respectively. Here, too, to a first approximation, the relation may be considered a linear one.

TABLE I
Slope and Intercept of the (σ_F^2/E)-vs.-Pressure Curve

Material	Pressure medium	A_0	A_1	γ at atm. pressure, ($\times 10^{-5}$ ergs/cm^2)[a]
Polyimide	kerosene oil	1270	0.0170	2.25–4.50
Polysulfone	kerosene oil	660	0.0118	1.16–2.32
Polyfulsone	heptane	565	0.0111	1.02–2.04

[a] The values of γ calculated by assuming $2c = 0.05$–0.10 cm.

If the inherent flaw size is assumed to be independent of pressure, then γ will vary linearly with P. If, on the other hand, the intrinsic flaw size itself depends on the magnitude of pressure, then γ will not, in general, vary linearly with pressure. The values of γ at atmospheric pressure, given in Table I, have been calculated from eq. (1), assuming the intrinsic flaw size $2c = 0.05$–0.10 cm, values comparable to those noted by Berry[4] for another brittle polymer, poly(methyl methacrylate).

The values of γ obtained by the above procedure are comparable to those reported for a number of other glassy amorphous polymers.[4–6] However, as pointed out by Andrews,[7] Berry, [4,8,9] and Smith,[10] the observed values of γ are higher by several orders of magnitude than the theoretical values based on fracture of molecular bonds. The difference is associated with the large localized plastic flow that is accompanied by the fracture process. Such plastic deformation may arise from segmental chain motion and from chain orientation associated with stress concentration at the advancing crack tip. An important role may also be played by secondary van der Waal's forces. These are usually neglected in the theoretical treatment, but if considered, would give rise to a higher theoretical value for γ. It has also been reported that γ is a function of crack velocity,[4,5] strain rate,[6] magnitude of constant load,[7] and the ratio of craze length ahead of the crack tip to the inherent flaw size.[7]

In view of eq. (2), this would imply that the ratio γ/c is not a constant, but that it increases almost linearly with pressure, for both polymers. We may write

$$\frac{\gamma}{c} = A_0 + A_1 P \tag{3}$$

where A_0 and A_1 are material parameters that depend on the polymer and the pressure medium used. Values of these parameters, corresponding to the straight lines shown in the figures, are listed in Table I. To determine how γ or c itself varies with pressure, some additional assumptions or data are necessary.

Another reason for the observed values of γ to be high could be that, in Griffith's analysis, fracture surfaces are assumed to be smooth and normal to the applied tensile stress axis. However, in actual situations, the fracture surfaces are quite jagged and have many steps normal to and out of the fracture plane. The totality of this out-of-fracture-plane area gener-

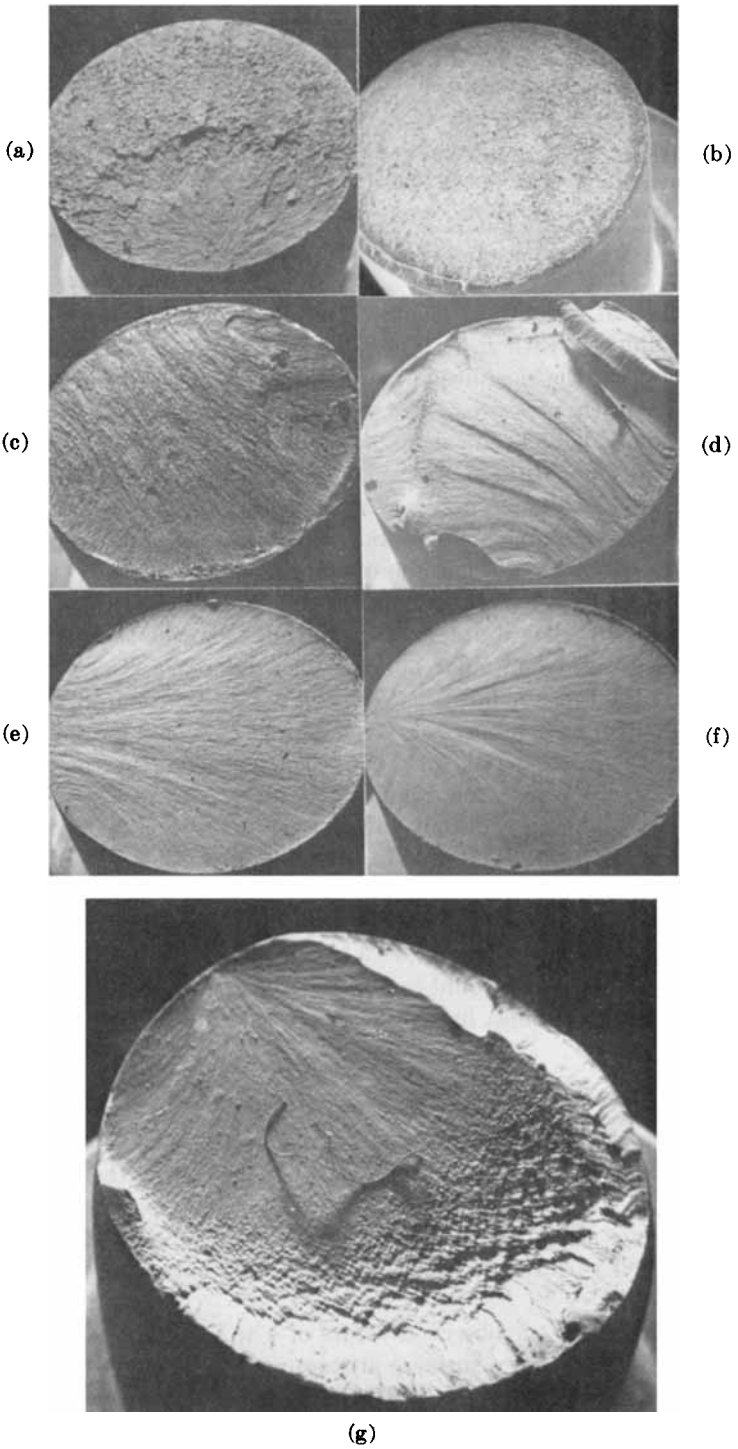

Fig. 10. Polyimide. Scanning electron micrographs (20×) of specimens tested at (a) atmospheric pressure (no oil); (b) atmospheric pressure; (c) 20,000 psi; (d) 40,000 psi; (e) 60,000 psi; (f) 80,000 psi; (g) 100,000 psi.

ated during fracture, if taken into account in Griffith's analysis, would also lead to lower values of γ.

It has been observed[9,11,12] that a decrease in temperature results in an increase in γ. However, in so far as mechanical properties are concerned, a decrease in temperature at atmospheric pressure produces a somewhat similar effect to an increase in pressure at room temperature. Hence, it is not surprising that in polymers, γ is found to increase with increasing pressure. The analogous behavior between lowering temperature and raising pressure is attributed to the common effect of both variables in decreasing the free volume and increasing the molecular interaction forces. In view of the reduced molecular mobility due to these two factors, a greater amount of work is required, at higher pressures, to create new surfaces, and hence the surface energy γ increases with increase in pressure.

Fracture Surface Studies by Scanning Electron Microscopy

To better understand the nature of the fracture process, and also to investigate the possible effects of pressure intensity and of the pressure medium on the fracture process, many fracture surfaces of tested tensile specimens have been studied by the use of a scanning electron microscope. The results of this study are presented below.

Polyimide

Figures 10a to 10g show scanning electron micrographs (20×) of the fracture surface of polyimide specimens fractured at the different superimposed hydrostatic pressures indicated on the figures. The primary fracture seems to initiate at some localized flaw or surface inhomogeneity within a region at the outer periphery of the specimen. The origin of fracture is quite evident, for example, in Figures 10a, 10f, and 10g. Figure 11

Fig. 11. Polyimide. Scanning electron micrograph (200×) of specimen tested at 80,000 psi.

shows a more detailed view (200×) of the fractured surface near the region of crack initiation for the 80,000-psi specimen. For the specimen tested at atmospheric pressure at ambient conditions in the Instron testing machine, fracture starts from a source, as Figure 10a shows. However, for a

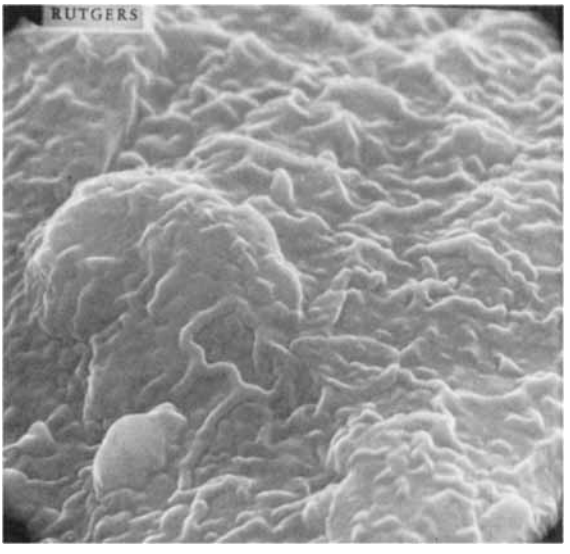

Fig. 12. Polyimide. Scanning electron micrograph (8000×) of specimen tested at 100,000 psi.

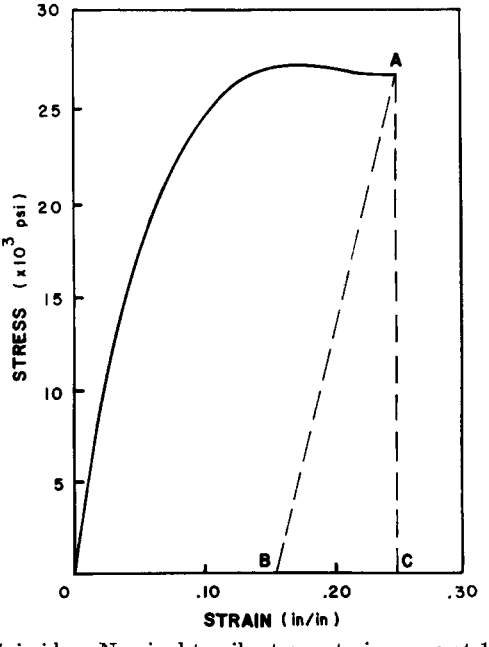

Fig. 13. Polyimide. Nominal tensile stress–strain curve at 100,000 psi.

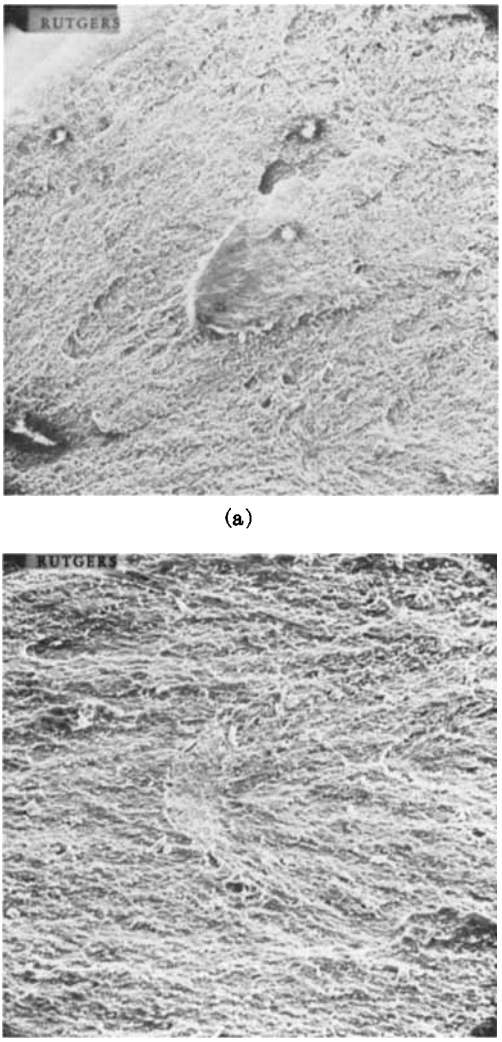

Fig. 14. Polyimide. Scanning electron micrographs of specimens tested at (a) atmospheric pressure (no oil) (160×); (b) 20,000 psi (120×).

corresponding specimen tested in kerosene oil, Figure 10b, the region of crack initiation is very broad possibly because of the growth of surface crazing regions. With increasing pressure as crazing is suppressed, the fracture again appears to develop from a point source, as Figures 10f and 10g show. At low pressures, say, up to 20,000 psi, the micrographs show that the fracture crack propagates along lines, termed orthogonal trajectories or radial traces,[13] emerging from the crack initiation source. At higher pressures, these orthogonal trajectories are more divergent, and the most divergent ones reach the periphery at a point nearer to the initiation

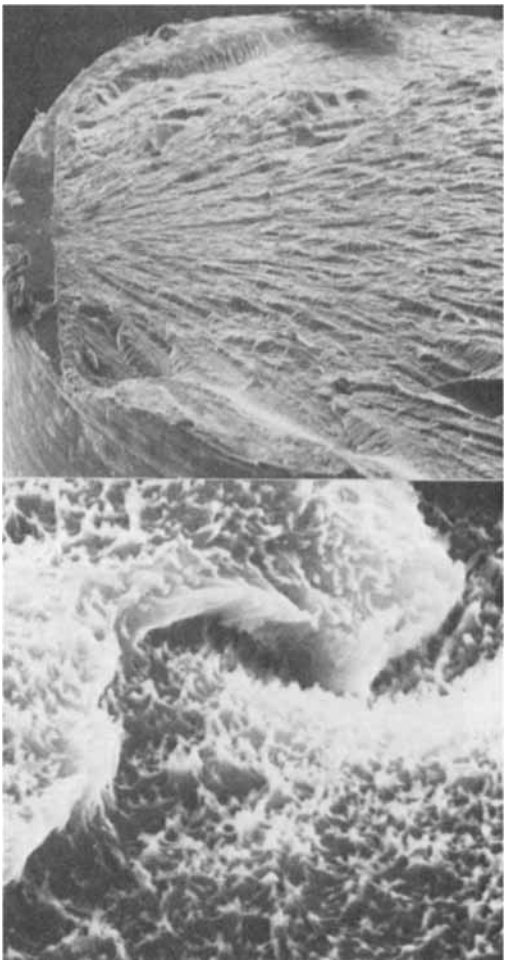

Fig. 15. Polyimide. Scanning electron micrographs of specimen fractured in liquid nitrogen at atmospheric pressure; (a) 100×; (b) 6000×.

point. The greater divergence of these radial traces, as the pressure is increased, may be a result of slower crack propagation with increasing pressure.

The increasing smoothness of the fracture surface with increasing hydrostatic pressure, as seen in Figure 10a to 10g, is itself an indication that a decrease in the rate of crack propagation with increase in pressure is occurring. It is generally considered[14–16] that roughness of fracture surface is a measure of velocity of crack propagation, rough area corresponding to fast crack growth.

From the scanning electron micrographs, it appears that there is an abrupt change in the nature of fracture between 80,000 and 100,000 psi. It is interesting to note that this change manifests itself also in the nominal

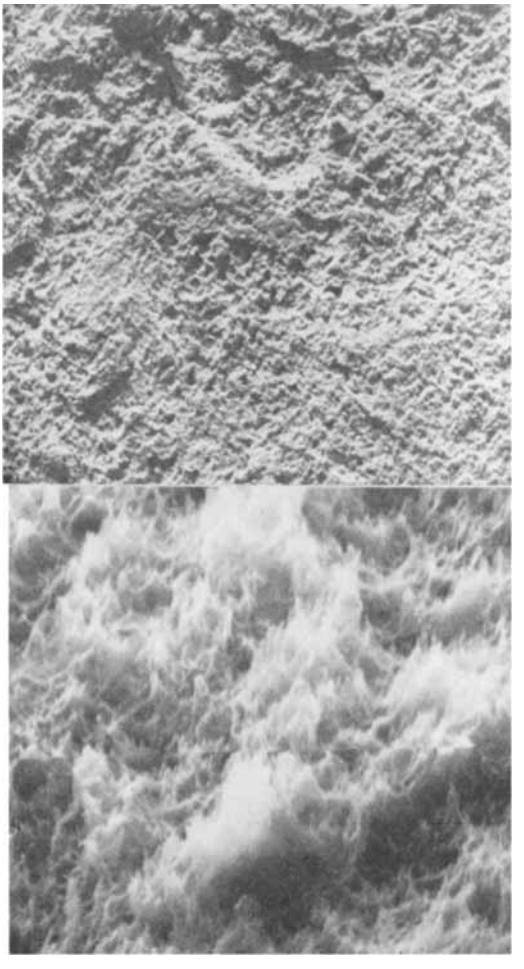

Fig. 16. Polyimide. Scanning electron micrographs of specimen tested at atmospheric pressure: (a) 200×; (b) 4000×.

stress–strain curves (Fig. 1) and in the geometry of the tested tensile specimens (Fig. 2). Whereas the 80,000-psi specimen (Fig. 10f) shows a smooth, mirror-like surface, the 100,000-psi specimen (Fig. 10g) shows three characteristic fracture surface areas usually referred to as the mirror region, the mist region, and the hackle region, respectively. As Figure 10g shows, the mirror area, the smooth region surrounding the crack initiation point, changes almost suddenly into a matt surface, referred to as mist, and finally into the roughest region, named hackle. In this final region, the crack propagates catastrophically in an irregular fashion owing to nucleation of numerous cracks and their bifurcation due to a change in stress distribution around the rapidly advancing crack,[17] thus giving rise to a very rough area.

Berry[4,8,9] has shown that fracture in polymers is accompanied by plastic deformation of a thin layer at the fracture surface, even when specimens

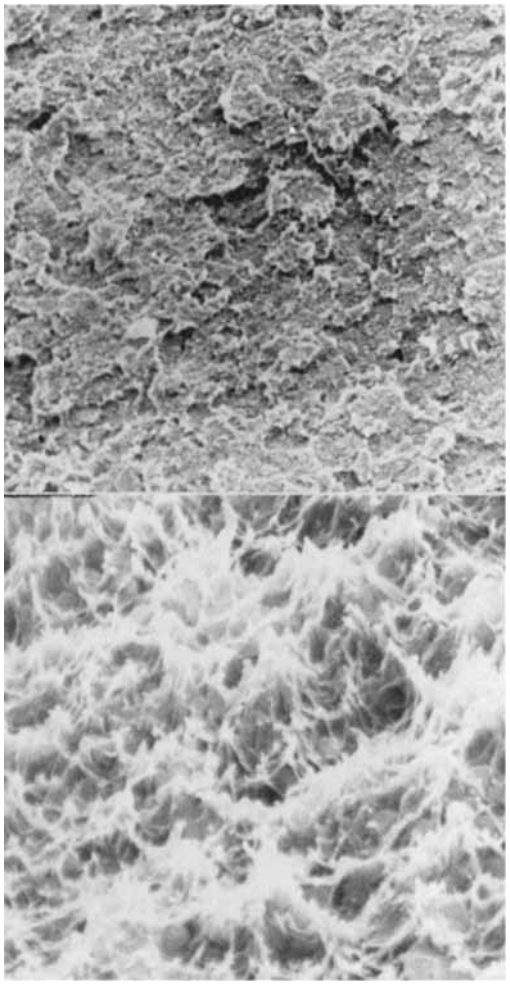

Fig. 17. Polyimide. Scanning electron micrographs of a specimen tested at atmospheric pressure: (a) 200×; (b) 8000×.

are tested at temperatures below their glass transition temperatures. Therefore, Bird et al.[18] have suggested that the fracture surface studies are likely to give information about the plastic deformation accompanying fracture, rather than about the true structure of the polymer under investigation. The 100,000-psi specimen, which does undergo a considerable plastic deformation, exhibits a worm-like fracture pattern (Fig. 12). It appears as if a thin layer of material were pulled out from the surface during deformation and relaxed later on with the passage of time. A similar situation may have occurred at other cross sections as well, thus giving rise to an appreciable overall plastic deformation prior to fracture.

It is appropriate at this point to inquire as to the expected temperature rise that one might get when the material fractures, as this will give some

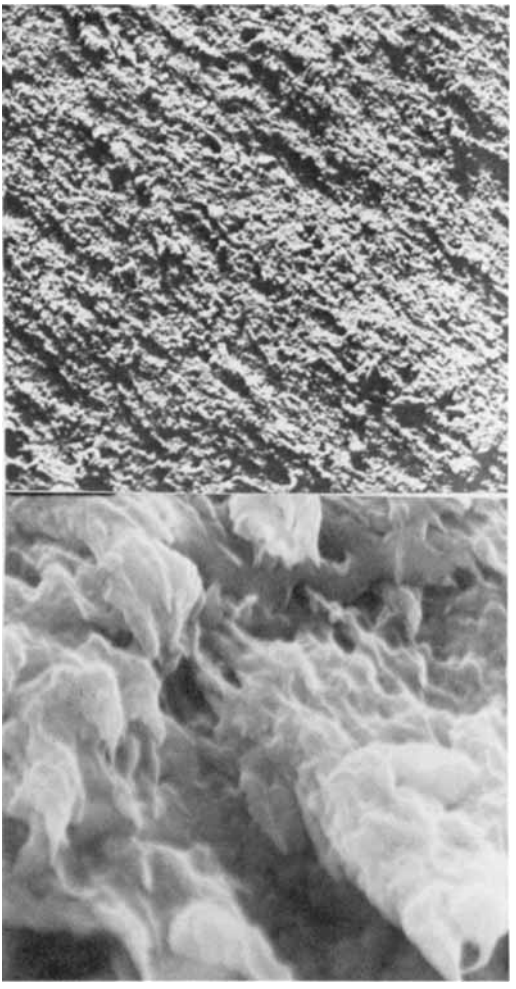

Fig. 18. Polyimide. Scanning electron micrographs of specimen tested at 20,000 psi: (a) 200×; (b) 8000×.

indication as to the importance of various processes in the fracture process. Consider the nominal tensile stress–strain diagram for the 100,000-psi specimen shown in Figure 13. The amount of temperature rise in the specimen associated with the fracture process can be roughly estimated from the stored elastic energy per unit volume, U_{rel}, released upon fracture. This energy is given by the triangular area ABC as follows:

$$U_{rel} = {}^1/_2\,(27{,}500)(0.10)\ \text{in.-lb/in.}^3$$

$$= 1375\ \text{in.-lb/in.}^3$$

$$= 0.1472\ \text{BTU/in.}^3$$

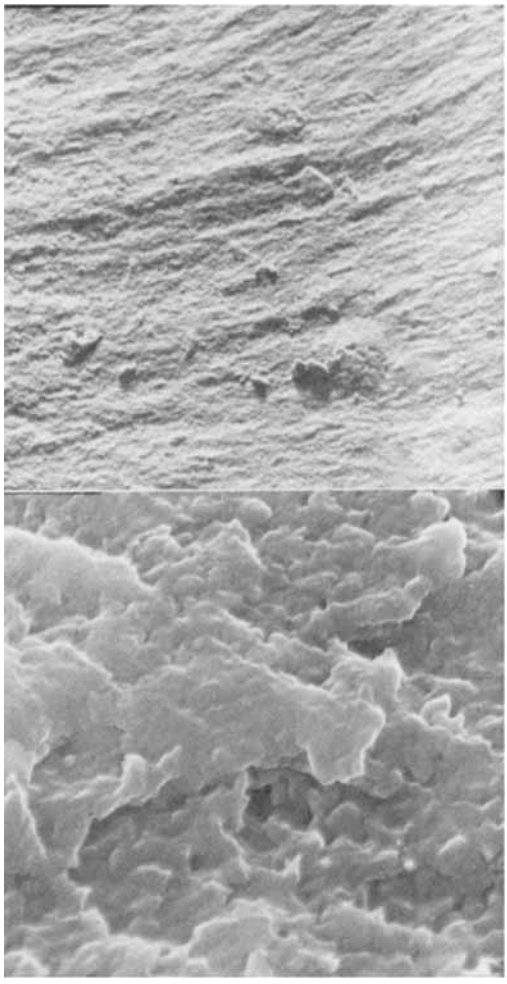

Fig. 19. Polyimide. Scanning electron micrographs of specimen tested at 60,000 psi: (a) 200×; (b) 8000×.

Assuming that this released energy goes to heat unit volume of material, we can write

$$U_{\text{rel}} = M \cdot C_p \cdot \Delta T \tag{4}$$

where M = mass of one cubic inch of material = $(1.43)\ (2.54)^3/453.6$ = 0.0517 lb/in.^{3}; and C_p = specific heat of the material = 0.27 BTU/lb $-$°F. Therefore, the temperature rise ΔT is given by

$$\Delta T = \frac{U_{\text{rel}}}{M \cdot C_P}$$

$$= \frac{0.1472}{(0.0517)(0.27)}$$

$$= 10.54°\text{F}.$$

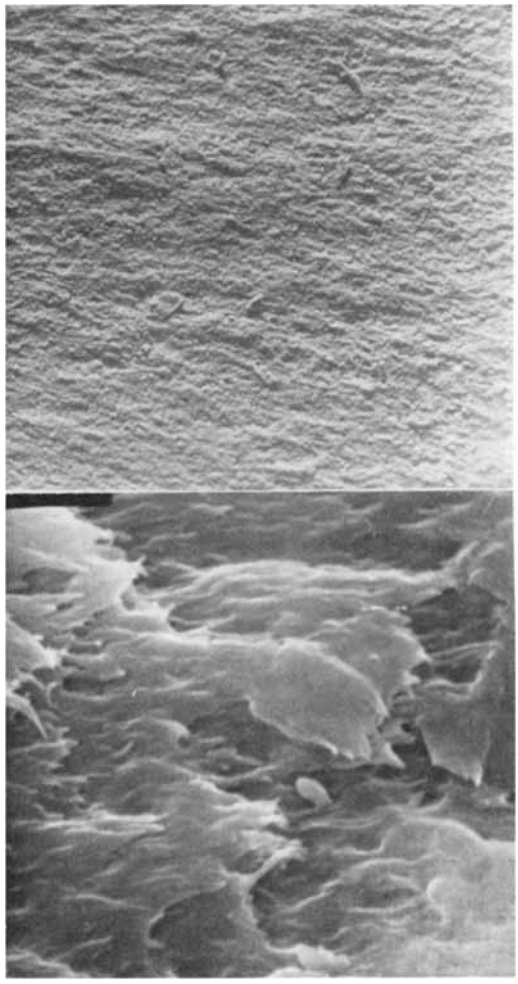

Fig. 20. Polyimide. Scanning electron micrographs of specimen tested at 80,000 psi: (a) 200×; (b) 8000×.

This calculation is based on the average value of applied tensile stress. However, the actual stress at the crack tip is k_1 times the overall stress, where k_1 is the stress concentration factor. For an Inglis-type elliptical crack,[19] it is given by

$$k_1 = 1 + 2(c_1/b_1)^{1/2} \tag{5}$$

where c_1 = length of an edge flaw = 2C, and b_1 = tip radius. The value of U_{rel} and hence at ΔT based on the localized maximum stress, therefore, becomes k_1^2 times the corresponding value based on the nominal stress. Thus, in a small volume in the neighborhood of a crack tip, one might expect a temperature rise of

$$\Delta T = 10.54 k_1^2 {}^\circ\mathrm{F}.$$

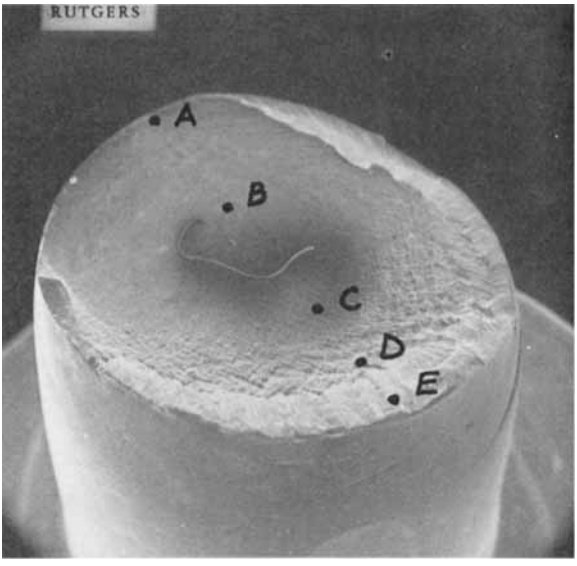

Fig. 21. Polyimide. Scanning electron micrograph (20×) of specimen tested at 100,000 psi.

The value of the stress-concentration factor k_1 can be as low as 3 for a smooth, circular hole in a thin plate and as high as 200 for an edge flaw about 10^{-3} cm long and about 10 Å in tip radius.[20] Thus, depending on the value of k_1, which is difficult to estimate precisely, the local temperature rise ΔT could be very high. For example, if k_1 is taken as 10, then the temperature rise $\Delta T = 1054°\text{F}$. While this value is unrealistically high, it is thought that the worm-like structures of Figure 12 and the globular entities to be seen later on in Figure 23b could arise from softening and subsequent vitrification after fracture of the material around the fracture plane.

During the fracture process, many secondary cracks are nucleated due to stress–concentration at inhomogeneities or flaws ahead of the primary fracture front. The interaction between a straight main crack front and a circular secondary crack front traveling on neighboring parallel planes results in fracture markings[21] which can be described by the following equation:

$$x^2(u^2/v^2 - 1) - y^2 = x_0\,(x_0 - 2x) \tag{6}$$

where x and y are the coordinates of a point on the generated fracture marking, x_0 is the initial distance between main fracture front and secondary fracture front, u is the radial velocity of secondary fracture front, and v is the velocity of primary fracture front.

If the primary and secondary fracture fronts are traveling with the same velocity (i.e., if $u = v$), then the fracture markings are quasi-parabolic. Such markings have been observed in the present study on the polyimide specimen fractured at atmospheric pressure and also on the specimen

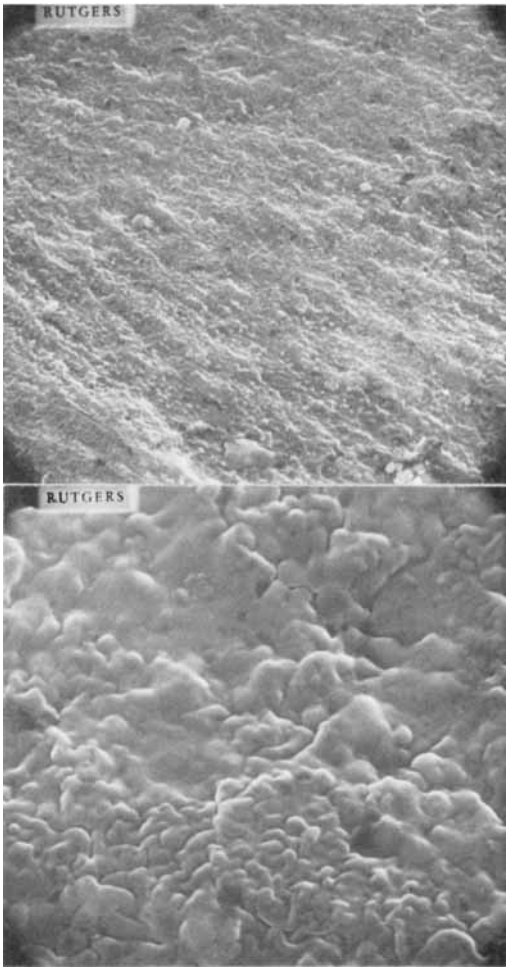

(a)

(b)

Fig. 22. Polyimide. Scanning electron micrographs of specimen tested at 100,000 psi, near point A (see Fig. 21): (a) 800×; (b) 4000×.

fractured at 20,000 psi, as shown in Figures 14a and 14b, respectively. The parabolic markings appear only on the specimens fractured at low-pressure values. The reason may be that at these low pressures the fracture velocity is much higher. There is always a good possibility that primary and secondary fractures will meet on slightly different planes a small distance apart, and when this occurs the fracture marking will be seen on the fracture surface. However, crack propagation at and above 40,000 psi is probably slow enough to let primary and secondary fractures adjust to meet on the same plane, thereby leaving no discontinuity to be seen on the micrograph. From the orientation of the fracture markings, it is generally possible to tell the direction of crack propagation. Parabolic fracture markings have been reported to occur in many different polymers.[18,22,23,24]

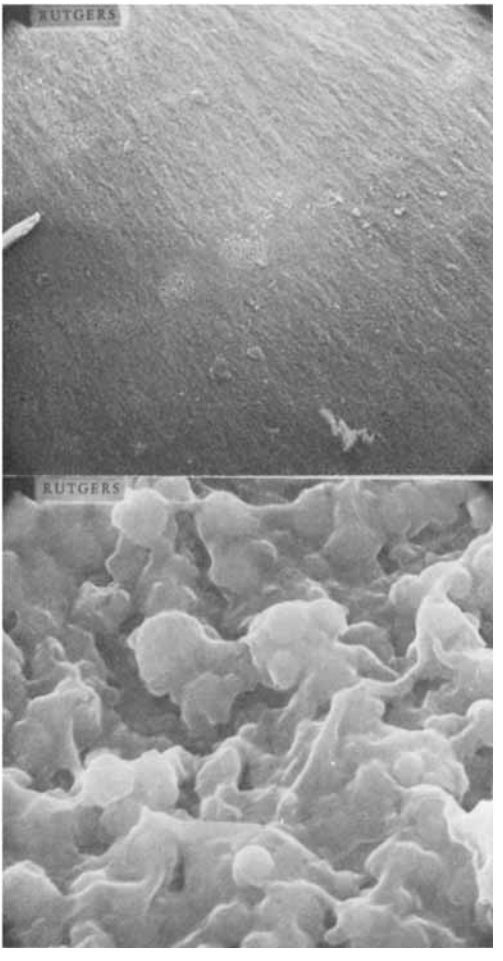

Fig. 23. Polyimide. Scanning electron micrographs of specimen tested at 100,000 psi, near point B (see Fig. 21): (a) 200×; (b) 4000×.

Figures 15 to 26 show typical scanning electron micrographs of fractured polyimide specimens tested in tension under varying superimposed hydrostatic pressures up to 80,000 psi. Pressures at which the specimens were tested and the magnifications at which the micrographs were taken are indicated under each micrograph. For comparison purposes, another polyimide specimen was fractured in liquid nitrogen. This specimen was given a fine razor blade cut in the middle and was supported with the cut facing down, in a container full of liquid nitrogen at atmospheric pressure. The specimen was then fractured by loading it in the center by a wedge and a hammer. This specimen, together with the other air pressure specimens tested in the Instron testing machine and in kerosene oil medium, all behaved macroscopically in a brittle manner; the nominal fracture strain for the latter two specimens, as noted earlier in this study, was 8–10%. How-

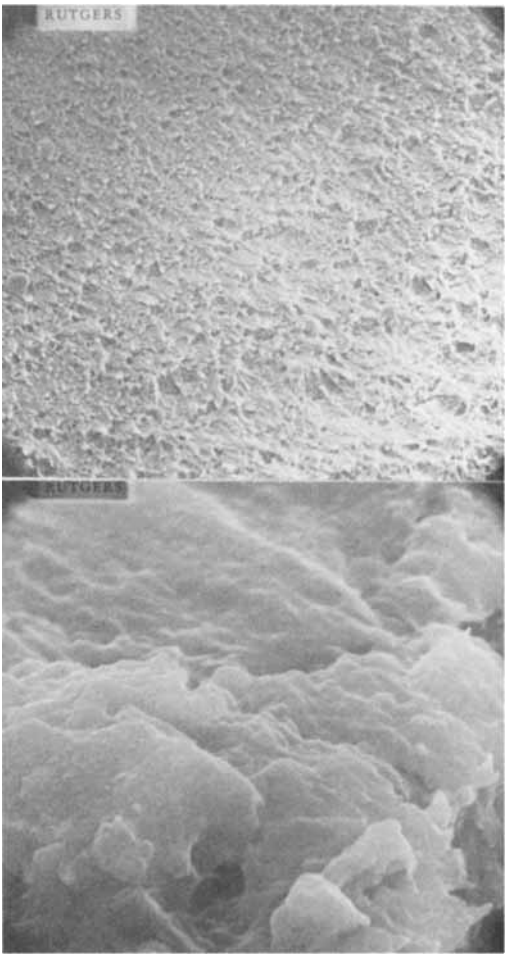

Fig. 24. Polyimide. Scanning electron micrographs of a specimen tested at 100,000 psi, near point C (see Fig. 21): (a) 200×; (b) 4000×.

ever, when examined with the scanning microscope, these specimens show large localized plastic deformation, as is evident from the fiber-like structure of Figures 15b, 16, and 17b. On comparing Figures 15b to 20b, it can be seen that the specimen texture becomes increasingly flat with increasing pressure although there are indications of the fiber-like texture being retained with fibers lying relatively flat, in all specimens up to 80,000 psi. The exact mechanism involved in the deformation at the microscopic level is not known at the present time.

As pointed out earlier in this investigation, the normally brittle polyimide becomes quite ductile at 100,000 psi. A neck develops and propagates in the gauge length, and the fracture strain increases to about 25%. It should thus be instructive to examine a 100,000-psi specimen (Fig. 21) in detail by a scanning electron microscope. To do this, scanning electron

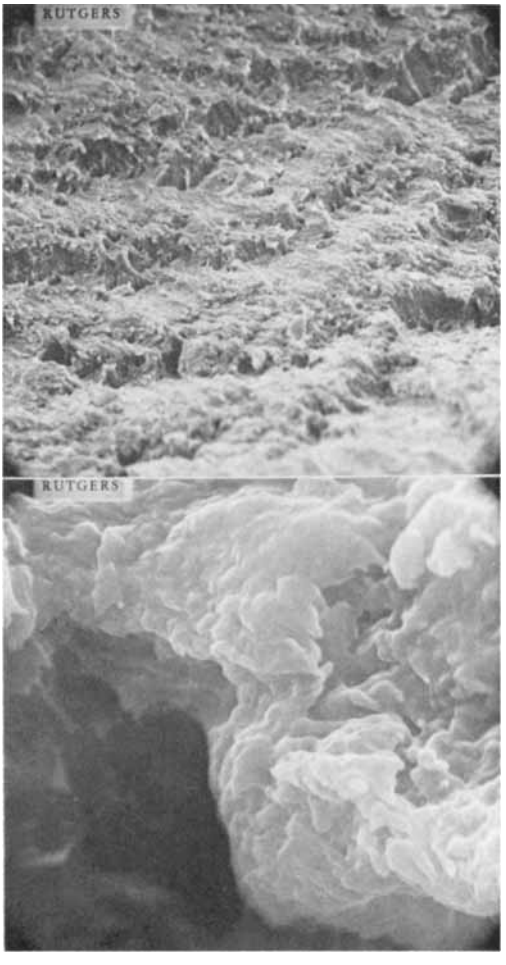

(a)

(b)

Fig. 25. Polyimide. Scanning electron micrographs of specimen tested at 100,000 psi, near point D (see Fig. 21): (a) 200×; (b) 4000×.

micrographs were taken at five different points, marked A, B, C, D, and E in Figure 21, along a line starting at the crack initiation point. Figures 22 to 26 show these micrographs at magnifications of 4000× and either at 200× or 800×, taken at each of the five points. A comparison of these micrographs indicates that the specimen surface becomes increasingly rough as we travel from the crack initiation point A in the mirror region to point E in the hackle region. Figure 22b shows the worm-like structure already noted to occur in Figure 26b. Figure 23b shows numerous globular entities. These could possibly arise due to "melting" and subsequent vitrification, after fracture, of the material in or around the fracture plane, if the specimen were heated enough locally by the elastic, stored energy released on fracture.

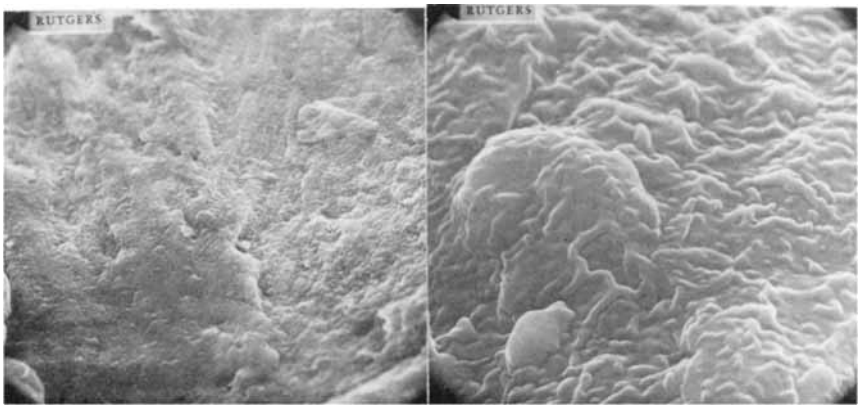

(a) (b)

Fig. 26. Polyimide. Scanning electron micrographs of specimen tested at 100,000 psi, near point E (see Fig. 21): (a) 800×; (b) 4000×.

Polysulfone

Figures 27a to 27b show scanning electron micrographs of fractured polysulfone specimens tested at different superimposed hydrostatic pressures with heptane as the pressure medium. Corresponding imicrographs for polysulfone tested with kerosene oil as the pressure medium are shown in Figures 28a to 28f.

The scanning electron micrographs reveal that there is a definite penetration of each pressure medium into the specimen surface up to a certain depth. This is clearly shown by the presence of an almost concentric ring visible to the naked eye, on the outer periphery of the fracture surface of almost all the heptane tested specimens and also the specimens tested at low pressure in kerosene oil. Such a ring, however, is absent on the specimens tested in the Instron testing machine in air at atmospheric pressure. This ring does not arise from faster cooling of the outer surface during original thermal extrusion, because the test specimens were machined down from original $^1/_2$-in.-diameter extruded rods to rods of 0.188-in. gauge diameter. In general, the thickness of the ring appears to be larger on the specimens tested in heptane than on specimens tested at corresponding pressures in kerosene oil. Furthermore, ring thickness seems to be almost constant with pressure for the specimens tested in kerosene oil. In fact, in the specimens tested in kerosene oil, the ring disappears at a pressure of about 40,000 psi.

The inside boundary of the ring appears to be a coalescence of a number of voids, as shown in Figure 29a for a 60,000-psi heptane specimen and Figure 29b for an 80,000-psi heptane specimen. One possible explanation is that the ring represents the depth to which crazes have developed prior to final fracture and that the pressure medium had penetrated into the craze voids. The holes visible on the micrographs may well result from the

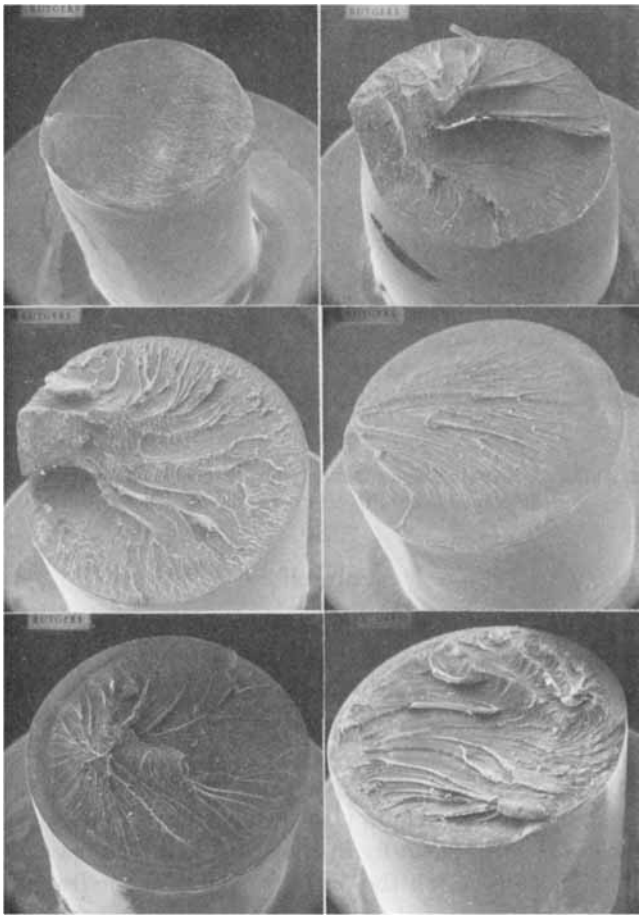

Fig. 27. Polysulfone. Scanning electron micrographs (20×) of specimens tested at (a) atmospheric pressure (no oil); (b) atmospheric pressure; (c) 20,000 psi; (d) 40,000 psi; (e) 60,000 psi; (f) 80,000 psi (all in heptane).

initiation and coalescence of voids in the region ahead of the fracture crack tip. The high localized stresses at the crack tip may cause dilatation and cavitation as well as plastic deformation.

In general, the fracture surface of specimens tested in kerosene oil seems to be smoother and flatter than that of corresponding specimens tested in heptane, especially at higher pressures. This suggests a slower crack propagation for the specimens tested in kerosene oil. For kerosene oil specimens, the fracture surface appears to become smoother and flatter with increasing pressure, possibly as a result of suppression of the craze inducing tendencies of kerosene as the hydrostatic pressure is raised. Heptane, however, is a stronger stress-cracking agent, and the fractured heptane-tested specimens show more and larger voids than the corresponding samples tested in kerosene oil. It is possible that the craze propensity of hep-

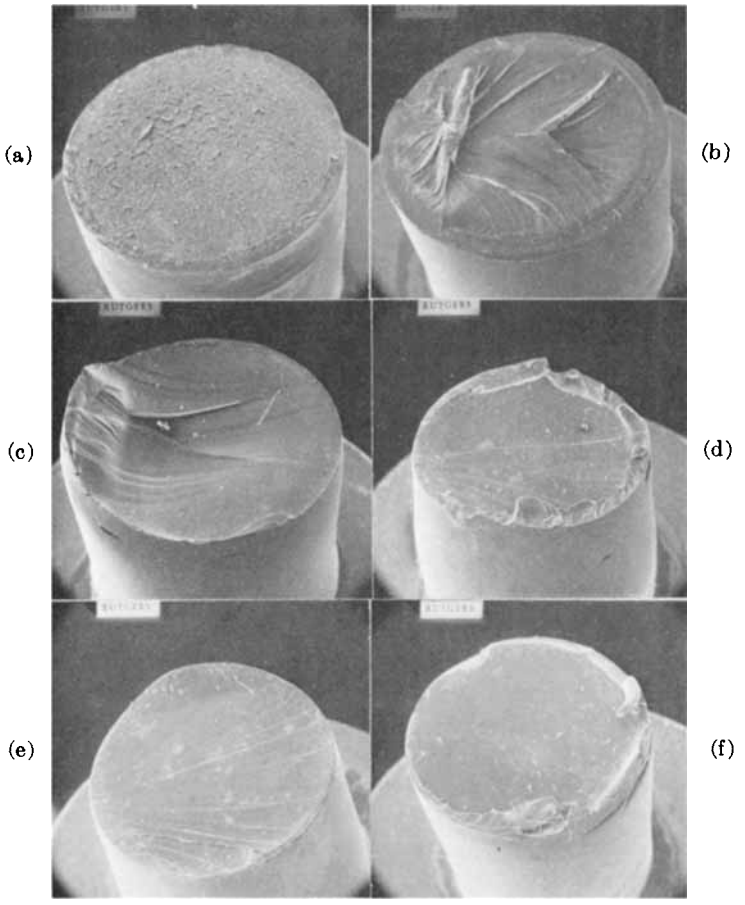

Fig. 28. Polysulfone. Scanning electron micrographs (20×) of specimens tested at (a) atmospheric pressure; (b) 20,000 psi; (c) 40,000 psi; (d) 60,000 psi; (e) 80,000 psi; (f) 100,000 psi (all in kerosene).

tane could also be overcome by hydrostatic pressure, but tests have not been made above 80,000 psi.

Figure 30, which shows a micrograph of a polysulfone specimen tested at 60,000 psi in kerosene oil, exhibits two or more sets of intersecting lines, the individual lines in each set being generally parallel to the other lines in that set. This may indicate that at this pressure level, shear-induced slip has occurred. A set of parallel lines, which again may be slip lines, was also observed in other specimens tested at higher pressures. That these bands are slip bands is supported by the observation of parallel oblique lines on the free surface of an 80,000-psi kerosene oil specimen when looked at under a light microscope. Further support comes from the fact that at and above 60,000 psi pressure, the specimens were observed to neck down in the tensile tests, which indicates that considerable yielding, slip, and localized high deformation has occurred in these specimens.

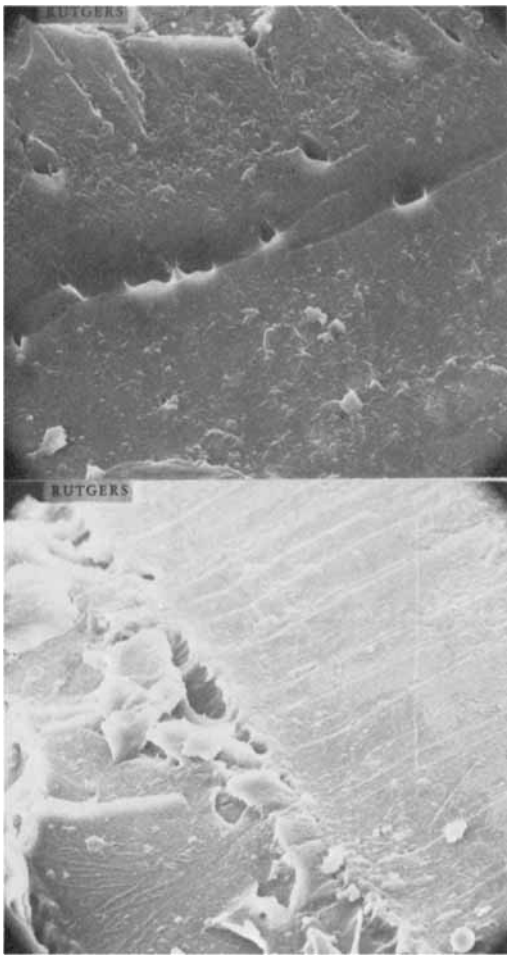

Fig. 29. Polysulfone. Scanning electron micrographs (800×) of specimens tested at (a) 60,000 psi; (b) 80,000 psi (both in heptane).

All the specimens tested in heptane show a river pattern of fracture, i.e., a primary crack initiating at some irregularity or inhomogeneity on or close to the outer periphery and then propagating along several different branches, each of which bifurcates further as the crack proceeds farther from the initiation point (Fig. 31). It is interesting to note that the edges of the quasiparabolic features have the appearance of a drawn structure which after fracture retracted considerably (Fig. 31). Similar phenomena have been observed by Bird et al.[25] in polystyrene.

In the case of one specimen tested in the Instron testing machine at atmospheric pressure, fracture was found to initiate at two different places almost diametrically opposite to each other (Fig. 27a). Both cracks, then, propagate away from their respective sources, with the crack fronts inter-

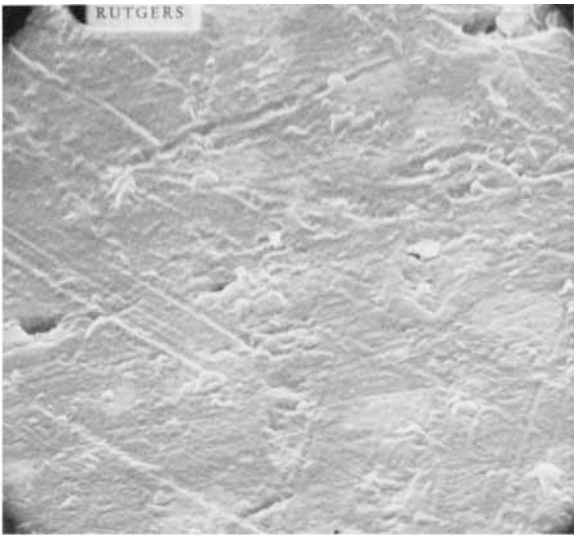

Fig. 30. Polysulfone. Scanning electron micrographs (4000×) of specimen tested at 60,000 psi (kerosene).

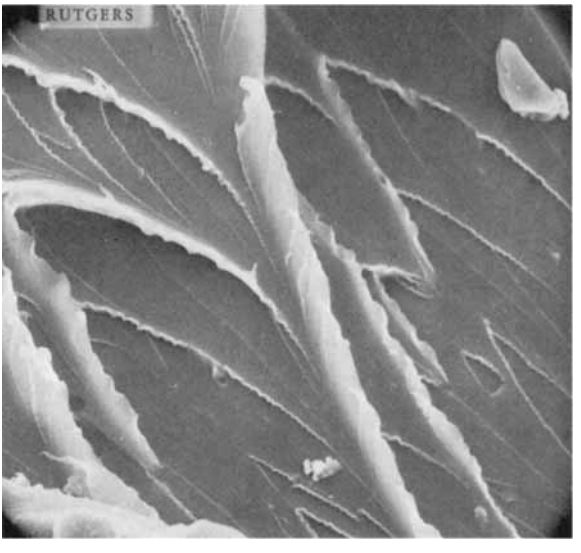

Fig. 31. Polysulfone. Scanning electron micrograph (800×) of specimen tested at 20,000 psi.

secting somewhere in between in a distinct line. As in the case of polyimide specimens, it is believed that the elastic, stored energy that is released on fracture may be sufficient to locally heat the specimen sufficiently high to cause small regions of the fracture surface to melt or soften and then subsequently to harden again or recrystallize. Adiabatic heating of the speci-

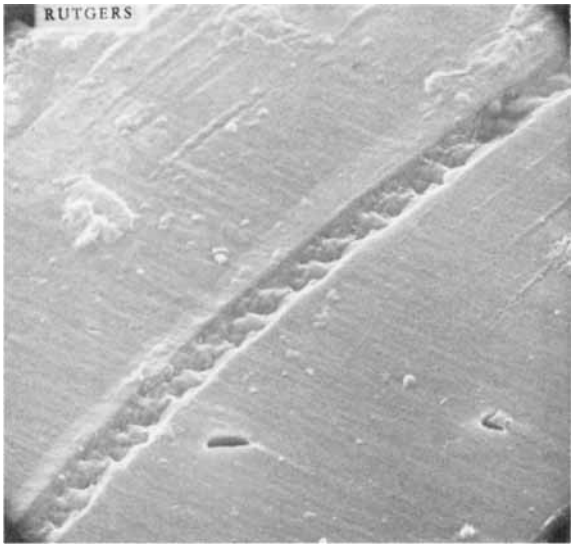

Fig. 32. Polysulfone. Scanning electron micrograph (4000×) of specimen tested at 100,000 psi (kerosene).

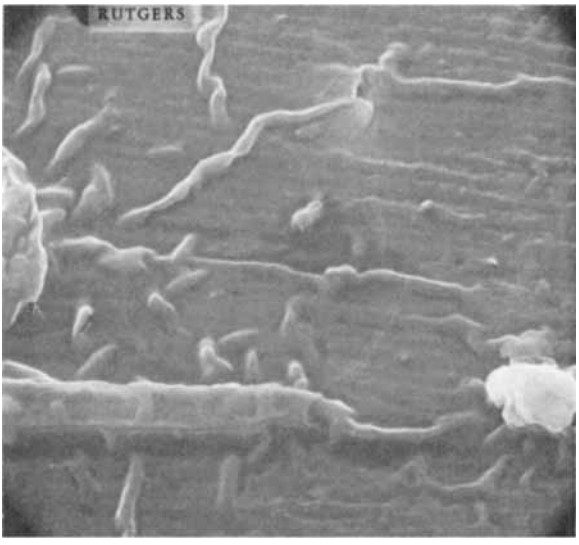

Fig. 33. Polysulfone. Scanning electron micrograph (4000×) of specimen tested at 100,000 psi (kerosene).

mens has been suggested before.[26] It is conceivable that the worm-like pattern of Figure 12 could arise from vitrification of such molten material.

The micrograph in Figure 32, corresponding to the specimen tested at 100,000 psi in kerosene oil, appears to show a crack with a set of ordered fibril bundles pulled across it. This may be the result of high localized

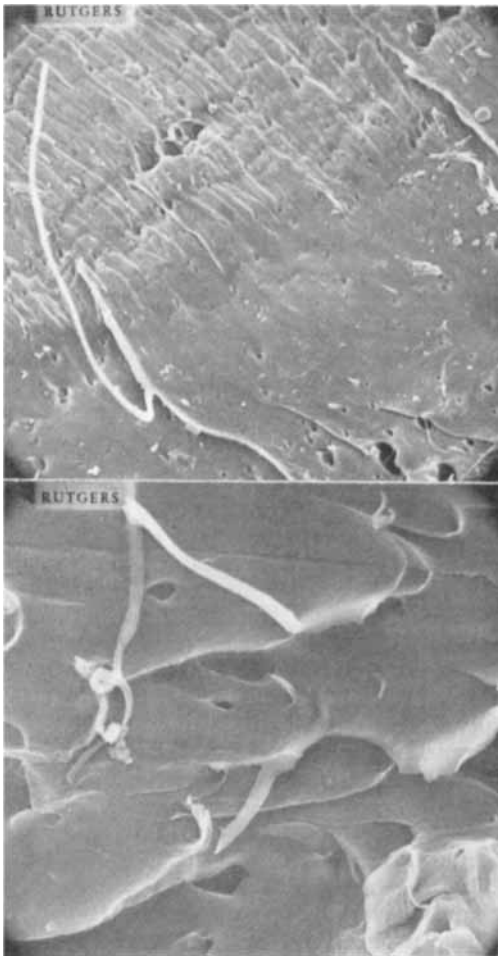

Fig. 34. Polysulfone. Scanning electron micrographs of specimens tested at (a) atmospheric pressure (200×); (b) 20,000 psi (800×) (both in heptane).

plastic deformation. It could be a result of a large temperature rise in the vicinity of a high localized stress region near an imperfection.

As in the case of polyimide, all the polysulfone specimens that did show high degree of plastic deformation also appeared to exhibit, at high magnification, a worm-like fracture pattern. This is the case for the 100,000 psi kerosene oil specimen shown in Figure 33.

Occasionally, long fibrils of the kind shown in Figures 34a and 34b were observed in some of the specimens tested in heptane. As pointed out by Bird et al.,[18] these are probably generated due to plastic deformation of the thin film of material that falls between the primary and secondary cracks which are traveling on two neighboring planes. Another possibility is that the fibrils represent material caught between the two fracture surfaces and considerably oriented (and subsequently retracted) prior to final fracture.

Figures 34a and 34b also show another common feature noted on many fracture surface micrographs of polysulfone. This is that the material is not homogeneous and that many holes or voids are present on the fracture surface. While some of these may be associated with initiation and coalescence of voids generated in front of the advancing crack tip, many of them are probably present in the original untested specimens. These voids may well arise from the original extrusion operation of the material into $^1/_2$-in.-diameter rod and from the presence of air bubbles or water vapor in the polymer powder.

The authors wish to thank the National Science Foundation and the Army Research Office–Durham for the financial support for this work. Also, the helpful assistance of Dr. J. W. Rue in the scanning electron microscope studies is greatly appreciated.

References

1. S. K. Bhateja and K. D. Pae, *J. Polym. Sci. B*, **10**, 531 (1973).
2. J. A. Sauer, S. K. Bhateja, and K. D. Pae, Proceedings of 3rd International Conference on Mater. Tech., Rio de Janiero, 1972, p. 486.
3. K. D. Pae, S. K. Bhateja, and J. A. Sauer, IUPAC Symposium on Macromolecules Preprints, **4**, Sec. III, 1972, p. 259.
4. J. G. Williams, J. C. Radon, and C. E. Turner, *J. Polym. Eng. Sci.*, **8**, 130 (1968).
5. G. P. Marshall, L. E. Culver, and J. G. Williams, *Plast. Polym.*, **37**, 75 (1969).
6. J. Murray and D. Hull, *J. Polym. Sci. A2*, **8**, 1521 (1970).
7. J. Murray and D. Hull, *J. Mater. Sci.*, **6**, 1277 (1971).
8. J. P. Berry, *J. Polym. Sci.*, **1**, 107 (1961).
9. S. Rabinowitz, I. M. Ward, and J. S. C. Parry, *J. Mater. Sci.*, **5**, 29 (1970).
10. J. J. Benbow and F. C. Roesler, *Proc. Phys. Soc.*, **70B**, 201 (1944).
11. E. H. Andrews, *Fracture in Polymers*, Elsevier, New York, 1968.
12. J. P. Berry, *J. Polym. Sci.*, **1**, 313 (1961).
13. J. P. Berry, *J. Polym. Sci.*, **1**, 993 (1963).
14. T. L. Smith, *J. Polym. Sci.*, **32**, 99 (1958).
15. L. J. Broutman and F. J. McGarry, *J. Appl. Polym. Sci.*, **9**, 589 (1965).
16. A. T. DiBendetto and K. L. Trachte, *J. Appl. Polym. Sci.*, **14**, 2249 (1970).
17. J. Gramberg, *Eng. Geol.*, **1**, 31 (1956).
18. I. Walock, J. A. Kies, and S. B. Newman, Fracture Phenomenon in Polymers, in *Fracture*, B. L. Averback, D. K. Felman, G. T. Hahn, and D. A. Thomas, Eds., Wiley, New York, 1959, p. 250.
19. J. P. Berry, *Nature*, **185**, 91 (1960).
20. J. A. Sauer and C. C. Hsiao, *J. Appl. Phys.*, **21**, 1071 (1950).
21. E. H. Yoffe, *Phil. Mag.*, **42**, 739 (1951).
22. R. J. Bird, J. Mann, G. Pogany, and G. Rooney, *Polymer*, **7**, 307 (1966).
23. C. E. Inglis, *Trans. Inst. Naval Arch.*, **55**, 219 (1913).
24. A. N. Gent, *J. Mater. Sci.*, **5**, 925 (1970).
25. J. Leeuwerik and F. Schwarzl, *Plastica*, **8**, 474 (1955).
26. R. P. Kambour, *J. Polym. Sci. A-2*, **4**, 17 (1966).
27. S. B. Newmann and I. Wolock, *J. Res. Nat. Bur. Stand.*, **58**, 339 (1957).
28. J. Murray and D. Hull, *Polymer*, **10**, 451 (1969).
29. R. J. Bird, G. Rooney, and J. Mann, *Polymer*, **12**, 743 (1971).
30. J. Murray and D. Hull, *J. Polym. Sci. A-2*, **8**, 583 (1970).

Received July 13, 1973